Hindawi
Journal of Nanomaterials
Volume 2020, Article ID 7480367, 11 pages
https://doi.org/10.1155/2020/7480367

Research Article

Photodeposition of Ag Nanocrystals onto TiO_2 Nanotube Platform for Enhanced Water Splitting and Hydrogen Gas Production

Nur Aimi Jani,[1,2] Choonyian Haw,[3,4] Weesiong Chiu,[1] Saadah Abdul Rahman,[1] Poisim Khiew,[5] Yingchin Lim,[2] Roslan Abd-Shukor,[6] and M. Azmi. Abd. Hamid[6]

[1]*Low Dimensional Materials Research Center, Department of Physics, Faculty of Science, University Malaya, Kuala Lumpur 50603, Malaysia*
[2]*Faculty of Applied Sciences, Universiti Teknologi MARA, Shah Alam, 40450 Selangor, Malaysia*
[3]*School of Energy and Chemical Engineering, Xiamen University Malaysia, Selangor Darul Ehsan 43900, Malaysia*
[4]*College of Chemistry and Chemical Engineering, Xiamen University, Xiamen 361005, China*
[5]*Center of Nanotechnology and Advanced Materials, Faculty of Engineering, University of Nottingham Malaysia Campus, Jalan Broga, 43500 Semenyih, Selangor, Malaysia*
[6]*School of Applied Physics, Universiti Kebangsaan Malaysia, 43600 Bangi, Selangor, Malaysia*

Correspondence should be addressed to Weesiong Chiu; w.s.chiu@um.edu.my

Received 21 January 2020; Revised 30 March 2020; Accepted 1 April 2020; Published 7 May 2020

Academic Editor: Ping Xiao

Current work reports the study of Ag nanocrystals (NCs) decorated doubly anodized (DA) TiO_2 nanotubes (NTs) thin film as an efficient photoelectrode material for water splitting and photocatalytic hydrogen gas production. DA process has been shown to be capable of producing less defective NTs and creating additional spacious gaps in between NT bundles to allow efficient and uniform integration of Ag NCs. By employing photoreduction method, Ag NCs can be deposited directly onto NTs, where the size and density of coverage can be maneuvered by merely varying the concentration of Ag precursors. Field emission scanning electron microscope (FESEM) images show that the Ag NCs with controllable size are homogeneously decorated onto the walls of NTs with random yet uniform distribution. X-ray diffraction (XRD) results confirm the formation of anatase TiO_2 NTs and Ag NCs, which can be well indexed to standard patterns. The decoration of metallic Ag NCs onto the surface of NTs demonstrates a significant enhancement in the photoconversion efficiency as compared to that of pristine TiO_2 NTs. Additionally, the as-prepared nanocomposite film also shows improved efficiency when used as a photocatalyst platform in the production of hydrogen gas. Such improvement in the performance of water splitting and photocatalytic hydrogen gas production activity can be credited to the surface plasmonic resonance of Ag NCs present on the surface of the NTs, which renders improved light absorption and better charge separation. The current work can serve as a model of study for designing more advanced nanoarchitecture photoelectrode for renewable energy application.

1. Introduction

The depletion of fossil fuel has triggered serious concern since crude oil reserves are vanishing at the rate of 4 billion tons a year [1]. Thus, it is predicted that oil deposits will be totally depleted by 2052 if consumption continues persistently at this rate [2]. Therefore, the development of a clean and renewable energy as alternative energy source without involving fossil fuel is a great technological challenge today. One of the realistic approaches is by adopting hydrogen gas as a recyclable energy carrier since it does not generate "greenhouse gas" during the combustion process. Moreover, it is clean, green, and renewable as well as has a large specific energy density to be converted into electricity in the fuel cell system for real-life usage. However, unfortunately, existing industrial hydrogen gas production still employs fossil fuels

(such as coal or natural gas), which emits a large quantity of carbon dioxide and consequently results in climate changes and acid rain [3].

With respect to this, hydrogen gas production using renewable energy resources rather than fossil fuels, such as photocatalysis water splitting process utilizing solar radiation, has attracted numerous interests for application as a clean energy carrier. Since the first breakthrough report by Fujishima and Honda on their success in designing photoelectrochemical (PEC) for producing hydrogen and oxygen gases through a water splitting process by using a TiO_2 electrode in 1972 [4], intensive efforts have been devoted in improving this process with the main objective of converting light energy into chemical energy by using renewable energy resources. Recently, semiconductor-driven photoelectrochemical water splitting has been identified as one of the ideal candidates in green and sustainable research for battling the global challenge of fossil fuel depletion as well as global warming. This technique has been recognized worldwide as an environmentally friendly method for hydrogen gas generation based on renewable and apparently unlimited natural resources such as water and solar energy [5].

In conjunction with this, congruent efforts have been devoted to improving the conversion efficiency of the process. Even though it has been more than three decades of explorative research on this technology, it still does not reach the commercialized status and research today is focused on the awareness of dilemma. The reasons are mainly due to the lack of feasible yet suitable approach in preparing high-quality photoelectrode thin film and lack of fundamental understanding on the factors that hamper photoelectrochemical performance. Basically, there are only a few parameters that dominate the controlled efficiency of the process, which influence the absorption spectrum, electron-hole separation efficiency, and photostability. With respect to these, TiO_2 renders the highest stability [6], is less carcinogenic [7], and is cost-effective [8]. Moreover, it is feasible to prepare a one-dimensional nanostructure (either in the form of nanowire, nanorod, or nanotube) for enhancement in light confinement, higher surface-active sites, efficient charge separation, and better carrier mobility properties. Among these nanostructures, nanotubes (NTs) are excellent candidates because they have a tubular structure and are easy to prepare in vertical aligned mode for better light trapping. It also can be anodized in a highly ordered tubular array to create a better surface-to-volume ratio [9]. Finally, the one-dimensional layout is well complemented for unidirectional electrical conduction and the curved tubular walls can promote efficient charge separation due to complementary carrier lifetime and carrier diffusion length [10].

Nevertheless, the bandgap energy of TiO_2 that lies in the UV-A region (380-400 nm) can suppress the overall performance of photoelectrochemical system because of the lower concentration of photoexcitons. In order to resolve this limitation, numerous techniques have been employed to shift the light absorption spectrum towards the visible-light region that comprised of ~40% of incident solar spectrum. For instance, bandgap engineering through nonmetal doping [11, 12] and dye sensitization [13] has been adopted to narrow the bandgap energy towards the visible-light region. However, nonmetal doping has its drawback of suppressing the number of free carriers due to the presence of surface trapping sites due to the introduction of external elements that are noncommensurable onto the lattice sites [14]. In terms of dye sensitization, dyes serving as activation elements to trigger photoexcitation frequently undergo photobleaching and thus gradually reduce light absorption, which has an impact on the overall performance.

Lately, noble metal nanocrystals (NCs) such as silver (Ag), gold (Au), and platinum (Pt) have been used as cocatalysts and are decorated onto semiconductor nanostructures to boost the photoelectrochemical performance. The surface electron of these noble metals can absorb visible light and then undergoes collective oscillations. These so-called surface plasmon resonance (SPR) feature can serve as additional energy input (in the form of electromagnetic wave) to promote efficient charge separation by breaking energy bonds during the preformed photoexcitation (electron and holes) process. It is possible for the plasmon-excited hot electrons in these noble metal NCs to be injected into the conduction band of semiconductors [15]. As a result, additional electrons that play the role of carriers can be swept towards the external circuit and subsequently render better photoconversion efficiency as compared to that of pure semiconductors. In addition, these noble metal NCs reveal satisfactory stability against oxidation, necessitate only trace quantities [16], and are economically feasible (especially silver) [17].

With respect to the advantages in decorating noble metals onto semiconductor nanostructures as photoelectrode, this current work is envisaged to contribute to the existing platform of photoelectrochemical technology for better advancement in this field, where a value-added photoelectrode (Ag NCs-decorated TiO_2 NTs) is fabricated and studied systematically. Besides this, there are numerous other works on Ag NCs-decorated TiO_2 NTs reported. However, the main difference of the current work compared to other works is that this work employs UV-light-activated photodeposition method to directly reduce Ag^+ ion incorporated onto NTs, which is rarely reported. By merely varying the Ag precursor concentration, the density of coverage and distribution of Ag NCs photodeposited onto the surface of NTs can be tailored. In contrast to other decoration methods such as isometric impregnation [18] and coreduction [19], this method renders better controllability in terms of particle coverage density and size distribution. Furthermore, there is no further posttreatment required in the current method as compared to the thermal-assisted hydrolysis reduction technique previously reported by Liu et al. [20]. Additionally, both the structural and photocatalytic properties can be maneuvered by varying the concentration of Ag precursors, which is simple and does not require the use of a vacuum system such as in the physical vapor deposition method. The threshold of photoconversion efficiency for the most optimum sample (0.2 M Ag/DA-TiO_2) of 1.393% at 1.006 V (versus Ag/AgCl) is higher than the value reported by Wang et al. [11], who adopted a relatively sophisticated and pyrophoric preparation technique to hydrogen-doped 1D TiO_2 nanostructures. Finally, the as-prepared Ag-decorated TiO_2 NTs

can be used as a platform to produce hydrogen gas through water splitting reaction under the absence of voltage bias. The current work can be used as a platform of study to diversify the preparation technique to produce similar nanocomposite system for clean and renewable energy application for long-term sustainability.

2. Materials and Methods

2.1. Synthesis of Double Anodization (DA) TiO_2 Nanotube Template. Titanium foils (99.7% purity, 0.25 mm thick, and 10 mm × 20 mm) from Sigma-Aldrich were used for preparing doubly anodized TiO_2 nanotubes (NTs). Prior to first-round anodization, the foils were ultrasonically cleaned with acetone followed by ethanol for 15 minutes. Upon that, those foils were rinsed with deionized water and dried in an oven. The first-round electroanodization process was carried out in a conventional electrodeposition setup comprised of two electrodes under vigorous magnetic stirring at room temperature, in which titanium foil served as the anode (or working electrode) while platinum rod was employed as a cathode (or counter electrode). The distance between the anode and cathode was fixed at 30 mm throughout the reaction. The electrolyte used was ethylene glycol ($C_2H_6O_2$; Alfa Aesar, UK) containing 0.2 M ammonium fluoride (NH_4F; R&M Chemicals, UK) and 2 vol% water (H_2O). Consort Power Supply EV245 was used for the first electroanodization process by supplying a constant potential (40 V) for the duration of 30 minutes followed by subsequent sonication for 10 minutes in an ultrasonic bath to remove the first-round electroanodization NT products. Upon sonication, the preformed NTs were peeled off and left the basal foil that were subsequently used as template for the second-round electroanodization process at identical potential (40 V) for 180 minutes. After this, this so-called doubly anodized TiO_2 NTs (DA-TiO_2 NTs) were immediately rinsed with deionized water, air-dried, and annealed at the 350°C for 3 hours by using a proportional–integral–derivative controller oven (Lenton-WHT6/30/3216P1) with predefined temperature ramping rate (5°C/min) to scrupulously control the annealing temperature for transforming the doubly anodized TiO_2 NTs that existed in an amorphous phase into well-crystalline anatase TiO_2 NTs.

2.2. Loading of Argentum Nanocrystals onto Doubly Anodized TiO_2 Nanotubes. The argentum nanocrystal-decorated doubly anodized TiO_2 nanotubes (Ag NCs/DA-TiO_2 NTs) were prepared via photoreduction process by immersing the as-annealed doubly anodized TiO_2 NTs (DA-TiO_2 NTs) in an aqueous solution of $AgNO_3$ (0.02 M) containing ethanol for 24 hours. The mixtures were then irradiated with a UV irradiation chamber (UV-crosslinker-UVP-CL1000, Cambridge) with the light source from a high-pressure mercury lamp (power of 8 W and emission wavelength of 254 nm). The samples were fixed at an irradiation distance of 4.0 cm below the lamp. The average intensity of UV irradiance exposed to samples was measured to be ca. 100 μJ/cm^2. Upon 2 hours of irradiation, the as-synthesized Ag NCs/DA-TiO_2 NTs were then rinsed with deionized water repeatedly to remove unreacted $AgNO_3$ precursor and dried at room temperature. In order to obtain DA-TiO_2 NTs decorated with different density coverage of Ag NCs, a similar experiment was repeated by using different concentrations of $AgNO_3$ (0.02 M, 0.11 M, 0.20 M, and 1.10 M). Thereafter, the samples were named in accordance with the concentration of the $AgNO_3$ precursor as 0.02 M Ag NCs/DA-TiO_2, 0.11 M Ag NCs/DA-TiO_2, 0.2 M Ag NCs/DA-TiO_2, and 1.1 M Ag NCs/DA-TiO_2.

2.3. Characterization. The morphology and elemental composition of Ag NCs/DA-TiO_2 NTs were observed using a variable-pressure field emission scanning electron microscope (FESEM-Zeiss Supra 35) equipped with energy dispersive X-ray spectroscopy (EDX). For a better overview of NTs length and Ag NCs distribution, cross-sectional images were taken from the edge of scratched samples. The crystallinity and phase transition were identified by an X-ray diffractometer (XRD, Panalytical Empyrean) under powder scanning mode with the X-ray source of Cu-Kα radiation that emitted a wavelength of 0.154 nm (40 kV and 35 mA). The scan rate of 0.05°/s was employed within a 2-theta range of 20° to 80°. Diffuse reflectance spectroscopy (DRS) (Varian Cary-5000 coupled with integrating sphere) was used to measure the absorption of the sample in UV-visible range.

2.4. Photoelectrochemical Water Splitting. Typically, a quartz-made photocell (Pine Research Instruments, RRPG147) with a flat optical window (surface quality: 60-40 scratch-dig) was used to ensure the perfect collimation of light. The photoelectrochemical setup was comprised of a standard three-electrode system, where the as-prepared samples in the form of thin films were used as a working electrode and Ag/AgCl electrode as reference electrode while Pt rod was used as a counter electrode. All irradiation was performed with the light source of xenon lamp (300 W) with an air mass filter (AM 1.5G) to simulate the real sunlight condition (100 mWcm^{-2}). The electrolyte used is 1.0 M NaOH solution. Linear sweep voltammetry (LSV) was conducted by using potentiostat (Autolab Potentiostat: Metrohm-PGSTAT302N) with the scanning rate of 10 mV/s.

2.5. Hydrogen Gas Generation. In order to evaluate the feasibility of samples as an efficient photocatalyst material for chemical fuel generation, hydrogen generation test was conducted. The reaction was preceded by mixing 3 ml ethanol (as sacrificial agent) with 27 ml deionized water in a 40 ml test tube. A 300 W Xe arc lamp serving as a UV-visible light source was mounted with a beam turner (Newport 66245) and attached with a fin-like heat sink to dissipate excessive heat. The test tube was placed 5.0 cm away from the edge of the filter holder, and the light was perpendicularly focused onto the thin film samples that were held by a sample holder. During the photocatalytic reaction, the gasses evolved onto the headspace of test tube were pumped into sample loop and further quantified by using gas chromatography (GC-Agilent 7890A) under online monitoring mode. The gas was separated by using MS-5A and HayeSep Q columns and analyzed by a thermal conductivity detector (TCD) attached on the GC.

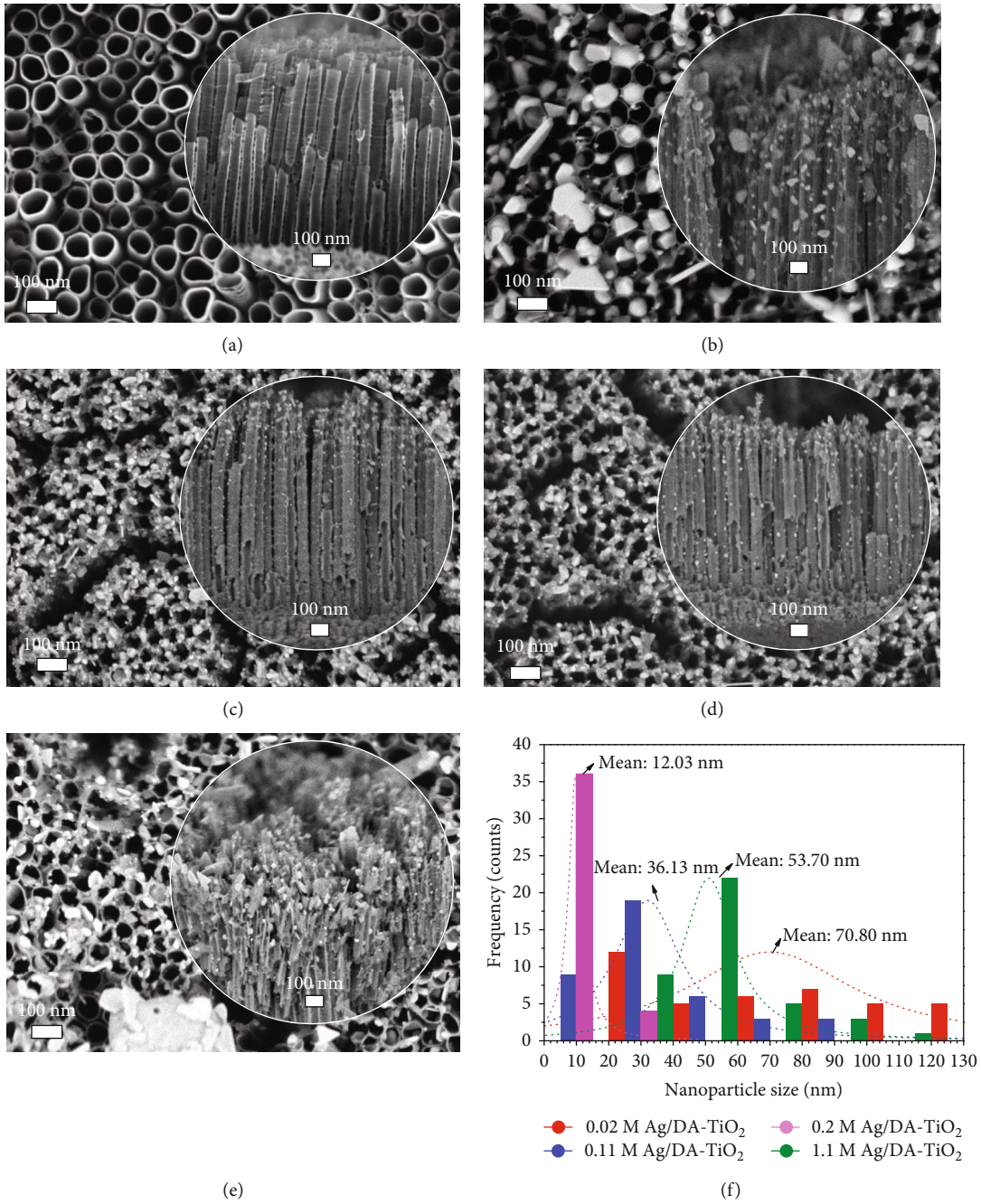

Figure 1: Top-view FESEM images at magnification of 50 kX for (a) pristine DA-TiO_2 NTs, (b) 0.02 M Ag/DA-TiO_2, (c) 0.11 M Ag/DA-TiO_2, (d) 0.2 M Ag/DA-TiO_2, (e) 1.1 M Ag/DA-TiO_2, and (f) size distribution histogram for the selected Ag NCs that decorated onto the surface NTs (inset spherical images in (a–e) is the cross-sectional view at magnification of 30 kX).

3. Results and Discussion

3.1. Morphological Study (FESEM). Figure 1 shows the cross-sectional and top view images (inset) as well as the size distribution of the as-prepared samples. According to the top-view image in Figure 1(a), doubly anodized pure TiO_2 nanotubes (DA-TiO_2 NTs) are having good monodispersity in terms of its internal diameter within the range of 150 nm to 160 nm and these NTs are well stacked together in relatively high packing order to form bundles. When referring to its cross-sectional image (inset Figure 1(a)), these NTs are well grown from the Ti substrate and indeed stacked together closely to each other with very limited space in between each NT. Somehow, these stacks of NTs reflect that each NT is not exactly vertically aligned. Instead, they appear to be slightly bended away from vertical orientation yet discontinue textures along its wall, which is having almost similar morphological appearance to that of TiO_2 NT membrane that was produced at higher voltage (60 V) by using graphite as a counter electrode [21].

For 0.02 M Ag/DA-TiO_2 NTs, it seems like there is not any major structural differences or morphological changes even though it had been integrated with Ag nanocrystals (NCs) as shown in Figures 1(b)–1(e). The difference is only in terms of the density coverage and morphological appearance of Ag with respect to the different concentrations of the Ag precursor. For the Ag precursor with a concentration of 0.02 M, a nonhomogeneous size of Ag NCs is randomly dispersed throughout the surface of DA-TiO_2 NTs as shown in the white-coloured spot in Figure 1(b). These Ag NCs have relatively broad and large size. This white-coloured spot is caused by an enhanced electron scattering phenomenon that is contributed by the abundance of surface electron in Ag NCs [22]. The size distribution analysis as depicted in Figure 1(f) indicates that the mean size of Ag NCs is estimated to be 70.80 nm (red-coloured graph). Furthermore, the morphology of Ag NCs appears to be ununiformed, where some of them appear to have irregular shapes ranging from an elongated structure up to multifaceted edges. These morphologies well agree with typical Ag nanostructures that are widely reported [23–25]. Such physical appearance with relatively large size and shape distribution is further supported by a cross-sectional image (inset image of Figure 1(b)), which reflects that the Ag NCs that anchored onto the wall of NTs are having rough yet granular surface topology.

For 0.11 M Ag/DA-TiO_2 NTs that had been prepared by increasing the concentration of the Ag precursor to 0.11 M, the mean size of NCs become smaller (Figure 1(c)) and the overall size distribution is improved and getting narrow as indicated in Figure 1(f). For this sample, it is found that most of the tiny Ag NCs are attaching onto the mouth edges of the NTs and some even go further deep into the internal compartment of the tube. The mean size of Ag NCs is found to be decreased down to 36.13 nm (Figure 1(f)). Meanwhile, the cross-sectional image (inset of Figure 1(c)) reveals that this sample has a smoother surface in contrast to the earlier sample, where some Ag NCs are successfully diffused through the bundle gap among the NTs and are attached onto the walls at one-third of the overall height from the top of NTs. In comparison to the existing study [26, 27], the NT bundles appear to be much more loosely packed to each other.

Moreover, for the sample that are grown with a Ag precursor concentration of 0.2 M (Figure 1(d)), there is no major variation as compared to that of 0.11 M Ag precursor concentration except in terms of Ag NC attachment along the vertical wall with respect to the cross-sectional view (inset of Figure 1(d)). However, the top-view image remains almost identical to that of 0.11 M Ag/DA-TiO_2 NTs (Figure 1(c)), whereby the Ag NCs is also randomly yet well dispersed at the mouth edges of NTs. The mean diameter is determined to be 12.03 nm with respect to Figure 1(f). It is predicted that a smaller size of NCs is beneficial for surface-enhanced plasmon resonance to take place [28, 29] and thus will enhance the photocatalytic performance in this study through improvement of the charge transfer rate and better electron-hole separation efficiency [30].

On the other hand, Figure 1(e) shows the FESEM image of 1.1 M Ag/DA-TiO_2 NTs, which are prepared by using a Ag precursor concentration of 1.1 M. According to the top-view image, the surface of some NTs is covered by Ag NCs with relatively large size distribution. Also, the shapes of Ag nanostructures appear to be slightly irregular. Moreover, part of NTs' mouth is fully blocked by these Ag NCs. As compared to the sample that is grown with a Ag precursor concentration of 0.2 M, the cross-sectional image of this sample reveals that the Ag NCs are highly agglomerated and densely occupying one-third of the top NTs' region. Such highly agglomerated Ag NCs are attributed to a homogeneous nucleation process that had taken place during the deposition of Ag^+ ion on DA-TiO_2 NT template. Due to the high concentration of Ag^+ ion, the saturation level easily gets attained and subsequently promotes the tendency of homogeneous nucleation among Ag nuclei itself [31]. This process occurs at a very fast rate and causes the nuclei that initially form in the solution to have no sufficient time to travel from the bulk solution to the surface of NTs. Instead, these nuclei further grow into highly agglomerated nanostructures with irregular shape rather than get deposited onto the surface of NTs. The mean sizes of the NCs for this sample are determined to be 53.70 nm.

3.2. Optical Study (DRS). The active absorption region for all the samples is identified by using diffuse reflectance spectra (DRS) and further converted into absorption spectrum. According to Figure 2, pristine DA-TiO_2 NTs reflect almost continuous yet negligible absorption in the visible light region. However, there is an obvious absorption that attributed to the excitonic electron transition from the valence band (O-2p orbital) to the conduction band (Ti-3d orbital) [32] at the UV region with the onset absorption ~375 nm. Upon Ag NC integration (sample 0.02 M Ag/DA-TiO_2), the onset absorption greatly shifted to ~600 nm, which implies that there is a traceable absorption in the visible-light region in addition to that of UV absorption at the bandgap energy transition point. The improvement on the light absorption can be ascribed to the so-called surface-enhanced plasmon resonance effects, which are contributed by collective oscillation of electron clouds on the surface of Ag NCs that are integrated onto the surface of NTs. This plasmon effect has been frequently reported to create a strong electric field that spreads towards its surrounding, which subsequently greatly improves electron-hole separation efficiency for those similar hybrid nanostructures that consisted of metal-semiconductor nanostructures [33–35]. Such improvement in electron-hole separation implies that the larger number of photoexcitation had taken place. Thus, an enhancement of absorption is observed in the UV region for all the Ag NC-integrated TiO_2 NTs in Figure 2.

With respect to the changes on the absorption for those samples that had been integrated with Ag NCs, it is found that there is progressive absorption with respect to the increment of Ag precursor concentration. Among all those samples, the sample prepared with a Ag precursor concentration of 0.2 M appears to own the most optimum absorption in the visible-light region. Further increment

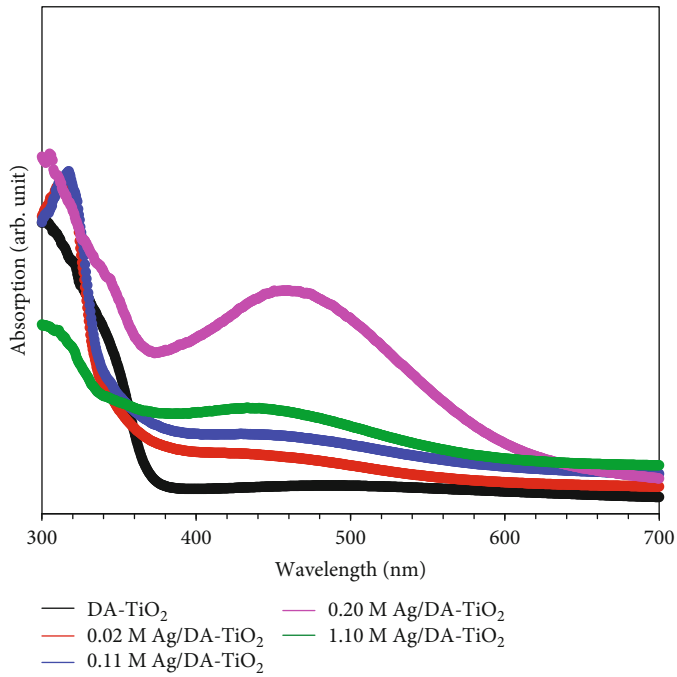

FIGURE 2: UV-Vis absorption spectrum of DA-TiO_2 NTs, 0.02 M Ag/DA-TiO_2 NTs, 0.11 M Ag/DA-TiO_2 NTs, 0.20 M Ag/DA-TiO_2 NTs, and 1.10 M Ag/DA-TiO_2 NTs.

on the Ag precursor concentration up to 1.1 M had resulted in the decrement on the absorption among all the Ag NC-decorated samples due to reduction on the quanta of light by larger-size NCs that attached on the surface of NTs. These larger-size NCs had render a screening effect by blocking large quanta of light from reaching to surface of TiO_2 to produce adequate number of excitons [36]. Hence, the light absorption for this sample is greatly suppressed.

3.3. Structural Study (XRD). Figure 3 shows the XRD patterns of the pristine DA-TiO_2 NTs annealed at 350°C for 3 hours and Ag NCs/DA-TiO_2 NTs with different Ag precursor concentrations for 0.02 M, 0.11 M, 0.2 M, and 1.1 M. For the spectra of DA-TiO_2 NTs, the peaks at 25.28°, 37.80°, 38.58°, 48.05°, 53.89°, 55.06°, and 62.68° are well matched to (101), (004), (112), (200), (105), (211), and (204) reflections of anatase phase, which are in well accordance with the standard pattern of JCPDS No. 21-1272. Meanwhile, the peaks at 2 theta of 38.11°, 44.28°, and 64.43° can be associated to the planes of (111), (200), (220), and (311), which belong to Ag with the cubic-phase crystal system (JCPDS NO. 04-0783). Upon integration, the relative intensity of the peak at 38.11° depicts an obvious increment as compared to that of pure DA-TiO_2 NTs. This reflects the successful decoration of Ag NCs without the alloy formation since there is not any unknown peaks or peak shifting presence. All these observations well complement to the XPS result that will be discussed in the following section.

3.4. Composition Study (XPS). In order to prove that the as-prepared TiO_2 NTs are indeed composed of pure anatase-phase TiO_2 (but not rutile-phase TiO_2) as well as to prove that the as-synthesized Ag NCs do not experience major oxidation, XPS is carried out on the representative sample of 0.2 M Ag NCs/DA-TiO_2 NTs. Figure 4(a) depicts the wide scanning profile for this sample with the binding energy within the range of 600 to 100 eV. The spectra showed pronounced featured signals of a Ag 3d state. In more detail, the narrow scan is carried out to clearly elucidate the binding energy for each element as well as the purity of the compounds (Figures 4(d)–4(d)). According to Figure 4(b), a dominant peak is observed at 530.5 eV, which corresponds to the energy state of O1s that belongs to lattice oxygen of TiO_2 [37]. On the other hand, the peaks at 459.2 eV and 465 eV in Figure 4(c) can be assigned to the energy state of $2p_{3/2}$ and $2p_{1/2}$ sourced from core levels of Ti 2p in anatase TiO_2 as reported by Xiao [38]. Finally, the peaks at 368 eV and 374 eV in the Ag 3d spectrum in Figure 4(d) originate from the energy state of Ag $3d_{5/2}$ and Ag $3d_{3/2}$ of pure metallic Ag, respectively [33].

As a short remark, all the above results reveal that the as-synthesized NTs are indeed a pure anatase-phase TiO_2 without the presence of rutile phase. Similarly, the Ag NCs that are decorated on this sample are indeed a pure Ag without the formation of oxide byproducts even though the posttreatment annealing is carried out at 350°C for 3 hours to transform the amorphous TiO_2 into well-crystalline anatase TiO_2. Furthermore, this result also proved that the as-adopted photoreduction method is a feasible method that can be adapted to produce pure metal NCs integrated hybrid nanostructures without the formation of unwanted byproducts such as metal oxide and without inducing any phase transition such as alloying [39].

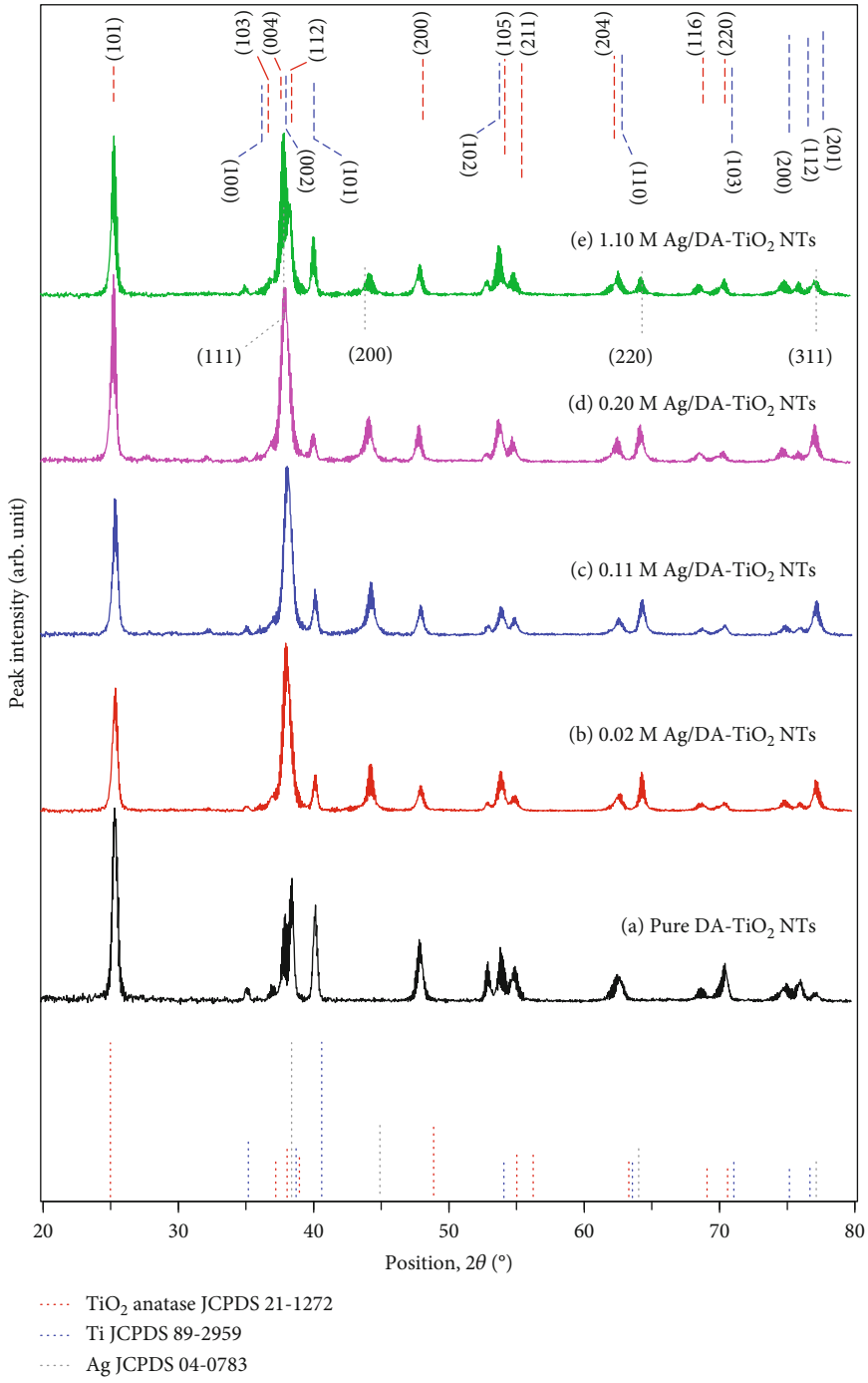

FIGURE 3: XRD patterns of (a) pristine DA-TiO_2 NTs, (b) 0.02 M Ag/DA-TiO_2, (c) 0.11 M Ag/DA-TiO_2, (d) 0.2 M Ag/DA-TiO_2, and (e) 1.1 M Ag/DA-TiO_2 (the solid and dashed lines at the bottom correspond to the standard pattern of TiO_2, Ti, and Ag, respectively).

3.5. Photoelectrochemical Water Splitting Study (LSV). The photoelectrochemical performance of Ag NCs/DA-TiO_2 NT heterostructure is shown in Figure 5. According to the linear sweep voltammetry (LSV) curve in Figure 5(a), the photocurrent density for pure DA-TiO_2 NTs is relatively low and the value is determined to be ~0.21 mA/cm^2. This value is well complemented with the values reported by other researchers [40–42]. Also, this value agrees well with the photocurrent density value that had been reported by Mohamed et al. [43], who had successfully produced ultrathin wall (4 nm in thickness) TiO_2 NTs for the first time and was used as a photoanode. The photoconversion efficiency (Figure 5(b)) for this sample is estimated to be 0.034% at a potential of 0.928 V (versus Ag/AgCl), which is relatively low.

Upon Ag NC integration, it is observed that the photocurrent density value increases in the range of 23 times (for sample 1.1 M Ag/DATiO_2) to 41 times (for sample 0.2 M

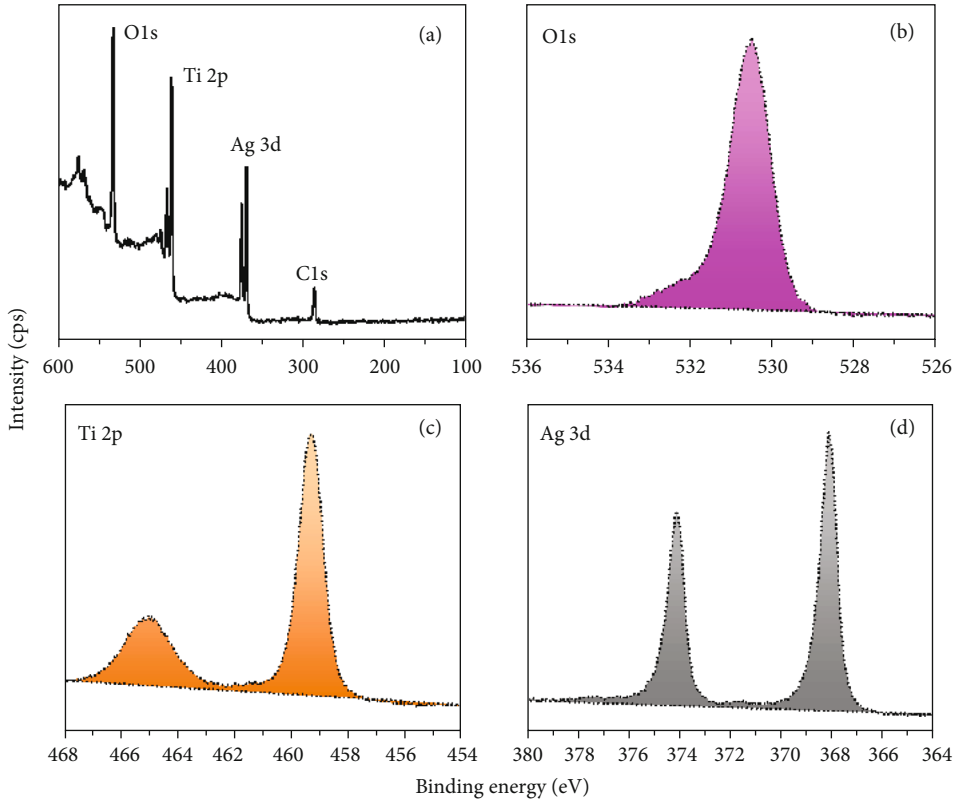

Figure 4: XPS scan spectra for 0.2 M Ag/DA-TiO_2. (a) Wide scan and narrow scan for (b) O1s, (c) Ti 2p, and (d) Ag 3d.

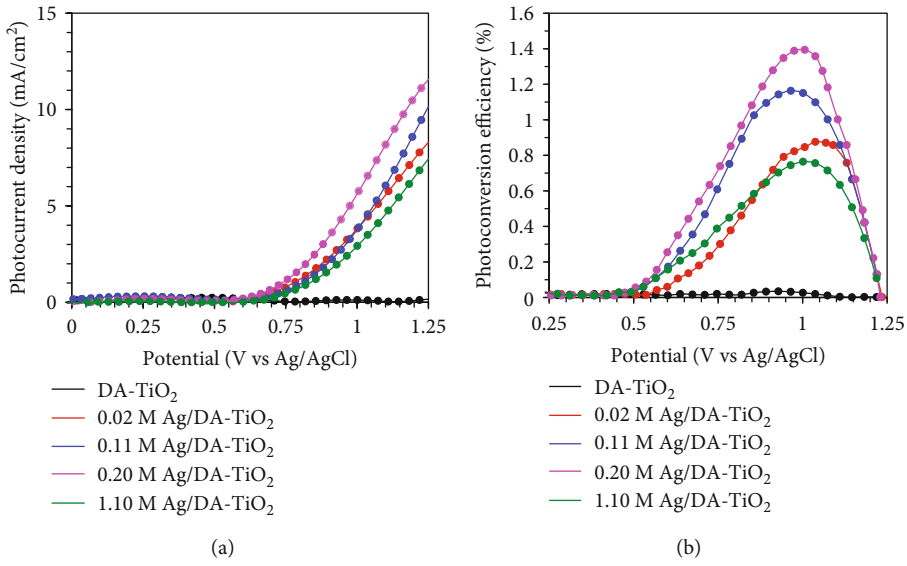

Figure 5: (a) Linear sweep voltammetry and (b) applied bias photoconversion for pristine DA-TiO_2 NTs, 0.02 M Ag/DA-TiO_2, 0.11 M Ag/DA-TiO_2, 0.2 M Ag/DA-TiO_2, and 1.1 M Ag/DA-TiO_2.

Ag/DATiO_2). The as-correlated photoconversion efficiency (Figure 5(b)) is found to increase to the range of 0.764% at 1.001 V (versus Ag/AgCl) for sample 1.1 M Ag/DATiO_2 to 1.393% at 1.006 V (versus Ag/AgCl) for sample 0.2 M Ag/DATiO_2. For all these Ag NC-decorated samples, significant photocurrent improvements are observed, where the photocurrent onset point begins to shift to more cathodic voltage. Similar cathodic shifting is also observed in photoconversion efficiency. The shifting towards cathodic potential can be attributed to the efficiency in band bending,

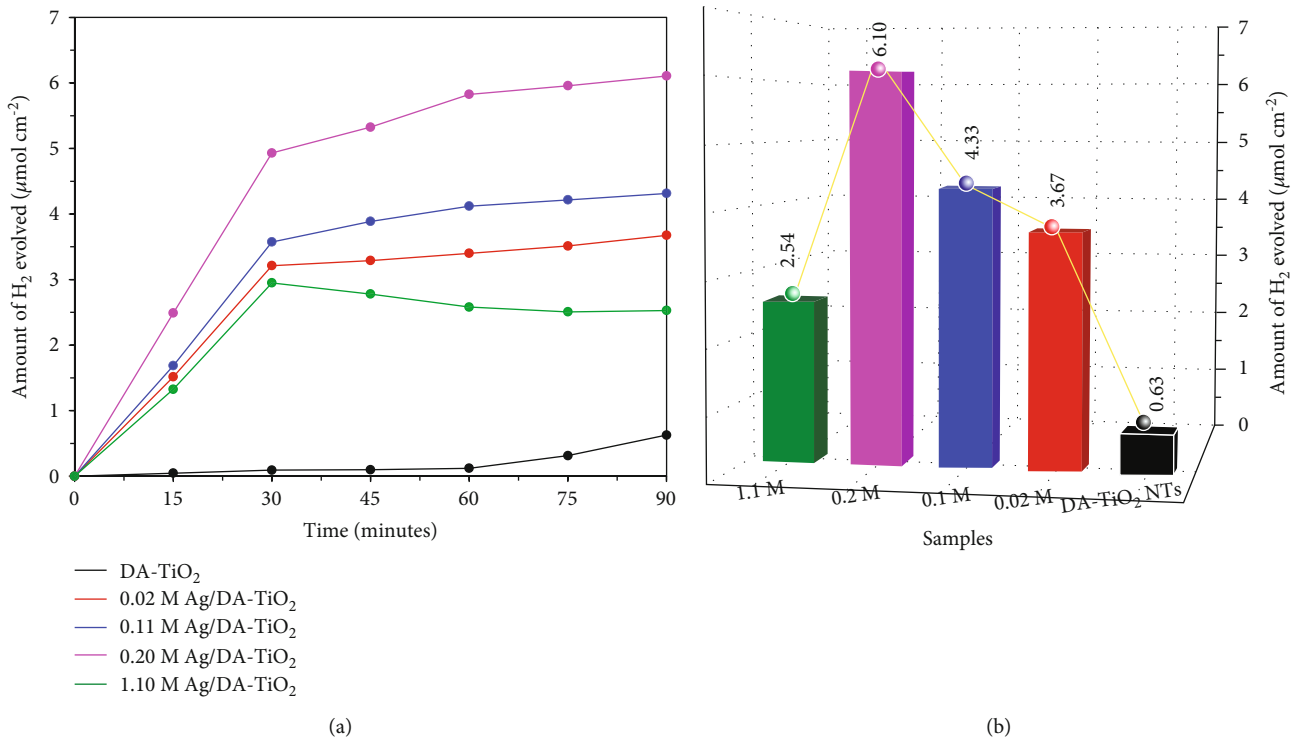

FIGURE 6: (a) Amount of hydrogen gas produced at specific time intervals (b) 3D bar chart of cumulative amount of hydrogen gas evolved at 90 minutes.

where a depletion region is created and produces an internal potential that is sufficient to separate the electron-hole pairs and produces higher photocurrent [44, 45]. Upon Ag NC decoration, it is deduced that a higher number of photoexcited electrons are produced because of surface plasmon resonance that is created by Ag NCs. The surface plasmon resonance that arises from collective oscillation of surface electrons on the surface of Ag NCs has spread towards the interface between Ag NCs and TiO_2 NTs. As a result, those photoexcited electrons manage to gain additional energy input to break the exciton binding energy and existed in the transient state as free carriers [27]. As a result, overall electron-hole recombination is refrained, and efficient charge separation has taken place for better photocurrent density output in all the Ag NC-decorated NTs.

3.6. Hydrogen Gas Generation Analysis. In order to evaluate the performance of the as-prepared samples to be used as photocatalyst platform for producing hydrogen gas, the samples are subjected to a similar lighting system in the section of photoelectrochemical test but without supply of any voltage. The hydrogen gas yield is obtained by normalizing to the sample area. Figure 6(a) represents the amounts of hydrogen gas evolved at specific irradiation time intervals. The amount of hydrogen gas produced by pristine TiO_2 NTs is estimated to be 0.63 μmol/cm^2 only at 90 minutes. Upon integration with Ag NCs, all the nanocomposite samples depicted a significant increment in hydrogen gas production rate as indicated in Figure 6(a).

The hydrogen gas production rate increased tremendously within the first 30 minutes, and the increment rates gradually reduced. Some fluctuations were observed for 1.1 M Ag/DA-TiO_2 NTs upon 30 minutes. Similar observation was also reported by Huang et al. [46], and they accredited such fluctuation to the presence of gas bubbles formed on the sample surface. These bubbles are believed to greatly suppress the probability of water molecules to get in contact with the sample surface and reduce the penetration of incident light needed for triggering the photoexcited electrons that are required for initializing the photocatalysis process. Nevertheless, the existence of bubbles is just temporary and they were diminished within a short time. Somehow, the new bubbles will form concurrently [47].

For better overview, a bar chart that reflects the cumulative amount of hydrogen gas produced at 90 minutes is plotted as shown in Figure 6(b), where the cumulative hydrogen gas yield for nanocomposites falls within the range of 2.54 μmol/cm^2 (for 1.1 M Ag/DA-TiO_2 NTs) up to 6.10 μmol/cm^2 (for 0.2 M Ag/DA-TiO_2 NTs). The progressive increment of the Ag precursor concentration indeed boosted the yield of hydrogen gas, and there was an optimum range of Ag precursor concentration up to 0.2 M. Further increment of the Ag precursor concentration rendered drawbacks by suppressing the photocatalytic activity as evidenced by sample 1.1 M Ag/DA-TiO_2 NTs. Such low yield of hydrogen gas is due to overoccupancy of Ag NC loading impeding the light from striking onto TiO_2 NTs. As a result, the numbers of photoexcited electrons generated on the surface of TiO_2 NTs are reduced and subsequently reduced the overall photocatalytic process as discussed in the aforementioned section.

4. Conclusion

As a conclusion remark, the direct photoreduction method has been successfully employed to integrate Ag nanocrystals (NCs) onto doubly anodized (DA) TiO_2 nanotube (NT) thin films and these thin films have been used as an efficient photoelectrode for applied bias water splitting. Additionally, its feasibility to be used as a photocatalyst thin film for hydrogen gas production has been evaluated. Detailed sample analysis reflects that the structural properties of the samples are strictly dependent on the Ag precursor concentrations used. The photocatalytic performance results also depict that there was an optimum Ag loading amount, where the 0.2 M Ag precursor concentration renders the best photocatalytic performance. The current study can serve as a platform that can be diversified to prepare a new type of hybrid-based nanomaterials, where noble metal can be directly photoreduced onto metal oxide semiconductor nanostructures for clean and renewable energy application.

Data Availability

All the data associated with results are plotted using Microsoft excel and complement with sigma origin to further enhance the visualization effect. Due to a large amount of raw data involved, hence, we will not include our raw data in current submission and we absolutely have no objection providing data upon further request.

Conflicts of Interest

The authors declare that they have no conflicts of interest.

Acknowledgments

This study was funded by Internal Research Grant (600-IRMI 5/3/LESTARI (030/2019)), Ministry of Education (FRGS: FP-038-2014B), and University Malaya Research Grant (UMRG-AFR Frontier Science-Project Number: RG390-17AFR). Additional financial support by Xiamen University Malaysia Research Fund (XMUMRF/2018-C1/IENG/0006) is highly appreciated. Khiew Poi Sim acknowledges the funding given by the Ministry of Education (FRGS/1/2019/STG02/UNIM/01/1). Nur Aimi Jani would like to thank the Ministry of Education (MOE) and Universiti Teknologi MARA for the SLAB/SLAI Ph.D. Scholarship as well as University of Malaya for the Postgraduate Research Fund (PG135-2014B).

References

[1] I. Hanif, S. M. Faraz Raza, P. Gago-de-Santos, and Q. Abbas, "Fossil fuels, foreign direct investment, and economic growth have triggered CO_2 emissions in emerging Asian economies: some empirical evidence," *Energy*, vol. 171, pp. 493–501, 2019.

[2] R. A. Barreto, "Fossil fuels, alternative energy and economic growth," *Economic Modelling*, vol. 75, pp. 196–220, 2018.

[3] S. A. M. Said, M. Waseeuddin, and D. S. A. Simakov, "A review on solar reforming systems," *Renewable and Sustainable Energy Reviews*, vol. 59, pp. 149–159, 2016.

[4] A. Fujishima and K. Honda, "Electrochemical photolysis of water at a semiconductor electrode," *Nature*, vol. 238, no. 5358, pp. 37-38, 1972.

[5] Y. Tachibana, L. Vayssieres, and J. R. Durrant, "Artificial photosynthesis for solar water-splitting," *Nature Photonics*, vol. 6, no. 8, pp. 511–518, 2012.

[6] S. Hamad, C. R. Catlow, S. M. Woodley, S. Lago, and J. A. Mejías, "Structure and stability of small TiO_2 nanoparticles," *The Journal of Physical Chemistry B*, vol. 109, no. 33, pp. 15741–15748, 2005.

[7] M. Skocaj, M. Filipic, J. Petkovic, and S. Novak, "Titanium dioxide in our everyday life; is it safe?," *Radiology and Oncology*, vol. 45, no. 4, pp. 227–247, 2011.

[8] M. A. K. L. Diasanayake, G. K. R. Senadeera, H. N. M. Sarangika et al., "TiO_2 as a low cost, multi functional material," *Materials Today: Proceedings*, vol. 3, pp. S40–S47, 2016.

[9] X. Chen and S. S. Mao, "Titanium dioxide nanomaterials: synthesis, properties, modifications, and applications," *Chemical Reviews*, vol. 107, no. 7, pp. 2891–2959, 2007.

[10] G. Hodes and P. V. Kamat, "Understanding the implication of carrier diffusion length in photovoltaic cells," *The Journal of Physical Chemistry Letters*, vol. 6, no. 20, pp. 4090–4092, 2015.

[11] G. Wang, H. Wang, Y. Ling et al., "Hydrogen-treated TiO_2 nanowire arrays for photoelectrochemical water splitting," *Nano Letters*, vol. 11, no. 7, pp. 3026–3033, 2011.

[12] S. Hoang, S. Guo, and C. B. Mullins, "Coincorporation of N and Ta into TiO_2 Nanowires for visible light driven photoelectrochemical water oxidation," *The Journal of Physical Chemistry C*, vol. 116, no. 44, pp. 23283–23290, 2012.

[13] P. Xu, T. Huang, J. Huang, Y. Yan, and T. E. Mallouk, "Dye-sensitized photoelectrochemical water oxidation through a buried junction," *Proceedings of the National Academy of Sciences of the United States of America*, vol. 115, no. 27, pp. 6946–6951, 2018.

[14] Z. Zhang, L. Zhang, M. N. Hedhili, H. Zhang, and P. Wang, "Plasmonic gold nanocrystals coupled with photonic crystal seamlessly on TiO2 nanotube photoelectrodes for efficient visible light photoelectrochemical water splitting," *Nano Letters*, vol. 13, no. 1, pp. 14–20, 2013.

[15] E. Rodríguez-Aguado, A. Infantes-Molina, A. Talon et al., "Au nanoparticles supported on nanorod-like TiO_2 as catalysts in the CO-PROX reaction under dark and light irradiation: effect of acidic and alkaline synthesis conditions," *International Journal of Hydrogen Energy*, vol. 44, no. 2, pp. 923–936, 2019.

[16] J. M. Buriak, C. Toro, and K.-S. Choi, "Chemistry of materials for water splitting reactions," *Chemistry of Materials*, vol. 30, no. 21, pp. 7325–7327, 2018.

[17] K. Sivula, "Toward economically feasible direct solar-to-fuel energy conversion," *The Journal of Physical Chemistry Letters*, vol. 6, no. 6, pp. 975-976, 2015.

[18] Y. Zhang, J. Bai, L. Zhou et al., "Preparation of silver-loaded titanium dioxide hedgehog-like architecture composed of hundreds of nanorods and its fast response to xylene," *Journal of Colloid and Interface Science*, vol. 536, pp. 215–223, 2019.

[19] S. N. H. Daud, C. Y. Haw, W. S. Chiu et al., "3D hyperbranched heterostructures of Ag nanocrystals-decorated ZnO nanopillars: controlled growth and characterization of the optical properties," *CrystEngComm*, vol. 19, no. 37, pp. 5591–5603, 2017.

[20] H. Liu, X. Dong, C. Duan, X. Su, and Z. Zhu, "Silver-modified TiO_2 nanorods with enhanced photocatalytic activity in visible

light region," *Ceramics International*, vol. 39, no. 8, pp. 8789–8795, 2013.

[21] H. Lv, N. Li, H. Zhang et al., "Transferable TiO_2 nanotubes membranes formed via anodization and their application in transparent electrochromism," *Solar Energy Materials and Solar Cells*, vol. 150, pp. 57–64, 2016.

[22] X. Wu, A. Centeno, X. Zhang et al., "Broadband plasmon photocurrent generation from Au nanoparticles/ mesoporous TiO_2 nanotube electrodes," *Solar Energy Materials and Solar Cells*, vol. 138, pp. 80–85, 2015.

[23] M. Grzelczak, A. Sánchez-Iglesias, H. Heidari et al., "Silver ions direct twin-plane formation during the overgrowth of single-crystal gold nanoparticles," *ACS Omega*, vol. 1, no. 2, pp. 177–181, 2016.

[24] Y. Sun, B. Mayers, T. Herricks, and Y. Xia, "Polyol synthesis of uniform silver nanowires: a plausible growth mechanism and the supporting evidence," *Nano Letters*, vol. 3, no. 7, pp. 955–960, 2003.

[25] B. J. Wiley, S. H. Im, Z. Y. Li, J. McLellan, A. Siekkinen, and Y. Xia, "Maneuvering the surface plasmon resonance of silver nanostructures through shape-controlled synthesis," *The Journal of Physical Chemistry B*, vol. 110, no. 32, pp. 15666–15675, 2006.

[26] X. Liu, X. E. Cao, Y. Liu, X. Li, M. Wang, and M. Li, "Branched multiphase TiO_2 with enhanced photoelectrochemical water splitting activity," *International Journal of Hydrogen Energy*, vol. 43, no. 46, pp. 21365–21373, 2018.

[27] L. Sang, H. Ge, and B. Sun, "Probing plasmonic Ag nanoparticles on TiO_2 nanotube arrays electrode for efficient solar water splitting," *International Journal of Hydrogen Energy*, vol. 44, no. 30, pp. 15787–15794, 2019.

[28] Y.-S. Chi, H.-P. Lin, and C.-Y. Mou, "CO oxidation over gold nanocatalyst confined in mesoporous silica," *Applied Catalysis A: General*, vol. 284, no. 1-2, pp. 199–206, 2005.

[29] Z. Hua, Z. Dai, X. Bai et al., "Copper nanoparticles sensitized TiO2 nanotube arrays electrode with enhanced photoelectrocatalytic activity for diclofenac degradation," *Chemical Engineering Journal*, vol. 283, pp. 514–523, 2016.

[30] C. Clavero, "Plasmon-induced hot-electron generation at nanoparticle/metal-oxide interfaces for photovoltaic and photocatalytic devices," *Nature Photonics*, vol. 8, no. 2, pp. 95–103, 2014.

[31] Y. Xia, Y. Xiong, B. Lim, and S. E. Skrabalak, "Shape-controlled synthesis of metal nanocrystals: simple chemistry meets complex physics?," *Angewandte Chemie International Edition*, vol. 48, no. 1, pp. 60–103, 2009.

[32] Y. Wang, R. Zhang, J. Li, L. Li, and S. Lin, "First-principles study on transition metal-doped anatase TiO_2," *Nanoscale Research Letters*, vol. 9, no. 1, p. 46, 2014.

[33] A. J. Cheah, W. S. Chiu, P. S. Khiew et al., "Facile synthesis of a Ag/MoS_2 nanocomposite photocatalyst for enhanced visible-light driven hydrogen gas evolution," *Catalysis Science & Technology*, vol. 5, no. 8, pp. 4133–4143, 2015.

[34] S. Linic, P. Christopher, and D. B. Ingram, "Plasmonic-metal nanostructures for efficient conversion of solar to chemical energy," *Nature Materials*, vol. 10, no. 12, pp. 911–921, 2011.

[35] Y. Sun, K. Liu, X. Hong et al., "Probing local strain at MX_2-metal boundaries with surface plasmon-enhanced Raman scattering," *Nano Letters*, vol. 14, no. 9, pp. 5329–5334, 2014.

[36] P. Spinelli and A. Polman, "Prospects of near-field plasmonic absorption enhancement in semiconductor materials using embedded Ag nanoparticles," *Optics Express*, vol. 20, Supplement 5, pp. A641–A654, 2012.

[37] J. Yu, G. Dai, and B. Huang, "Fabrication and characterization of visible-light-driven plasmonic photocatalyst $Ag/AgCl/TiO_2$ Nanotube arrays," *The Journal of Physical Chemistry C*, vol. 113, no. 37, pp. 16394–16401, 2009.

[38] F. Xiao, "Layer-by-layer self-assembly construction of highly ordered Metal-TiO_2 Nanotube arrays heterostructures (M/TNTs, M = Au, Ag, Pt) with tunable catalytic activities," *The Journal of Physical Chemistry C*, vol. 116, no. 31, pp. 16487–16498, 2012.

[39] X. Peng, M. C. Schlamp, A. V. Kadavanich, and A. P. Alivisatos, "Epitaxial growth of highly luminescent CdSe/CdS core/-shell nanocrystals with photostability and electronic accessibility," *Journal of the American Chemical Society*, vol. 119, no. 30, pp. 7019–7029, 1997.

[40] S. Hoang, S. Guo, N. T. Hahn, A. J. Bard, and C. B. Mullins, "Visible light driven photoelectrochemical water oxidation on nitrogen-modified TiO_2 nanowires," *Nano Letters*, vol. 12, no. 1, pp. 26–32, 2012.

[41] I. S. Cho, Z. Chen, A. J. Forman et al., "Branched TiO_2 nanorods for photoelectrochemical hydrogen production," *Nano Letters*, vol. 11, no. 11, pp. 4978–4984, 2011.

[42] Y. J. Hwang, C. Hahn, B. Liu, and P. Yang, "Photoelectrochemical properties of TiO_2 nanowire arrays: a study of the dependence on length and atomic layer deposition coating," *ACS Nano*, vol. 6, no. 6, pp. 5060–5069, 2012.

[43] A. M. Mohamed, A. S. Aljaber, S. AlQaradawi, and N. K. Allam, "TiO_2 nanotubes with ultrathin walls for enhanced water splitting," *Chemical Communications*, vol. 51, no. 63, pp. 12617–12620, 2015.

[44] M. Mollavali, C. Falamaki, and S. Rohani, "Efficient light harvesting by NiS/CdS/ZnS NPs incorporated in C, N-co-doped-TiO_2 nanotube arrays as visible-light sensitive multilayer photoanode for solar applications," *International Journal of Hydrogen Energy*, vol. 43, no. 19, pp. 9259–9278, 2018.

[45] T.-G. Vo, Y. Tai, and C.-Y. Chiang, "Multifunctional ternary hydrotalcite-like nanosheet arrays as an efficient co- catalyst for vastly improved water splitting performance on bismuth vanadate photoanode," *Journal of Catalysis*, vol. 370, pp. 1–10, 2019.

[46] Y.-C. Huang, S.-Y. Chang, and J.-M. Jehng, "Photocatalytic H_2 generation efficiencies of TiO_2 nanotube-based heterostructures grafted with ZnO nanorods, Ag nanoparticles, or Pd nanodendrites," *The Journal of Physical Chemistry C*, vol. 121, no. 35, pp. 19063–19068, 2017.

[47] K. Sun, Y. Jing, C. Li et al., "3D branched nanowire heterojunction photoelectrodes for high-efficiency solar water splitting and H_2 generation," *Nanoscale*, vol. 4, no. 5, pp. 1515–1521, 2012.